Internet of Things 30 (2025) 101486

Contents lists available at ScienceDirect

Internet of Things

journal homepage: www.elsevier.com/locate/iot

Research article

Unlocking the dynamic potential: Next-gen DOA estimation for moving signals via BSCS with adaptive weighted Kalman filter in 6G networks

Amgad A. Salama [a,b], Mahmoud A. Shawky [a,c], Samy H. Darwish [d], Adham A. Elmahallawy [e], Mohamed Abd Elaziz [f], Ahmad Almogren [g], Ahmed Gamal Abdellatif [a], Syed Tariq Shah [h,*]

[a] Department of Communications and Electronics Engineering, Air Defense College, EMA, Cairo University, Cairo, Egypt
[b] The Research and Development Center, ADC, Cairo, Egypt
[c] James Watt School of Engineering, University of Glasgow, G12 8QQ, Glasgow, UK
[d] Electrical Engineering Department, KMA-Academy, Alexandria, Egypt
[e] Higher Institute of Engineering and Technology, King Mariout, Alexandria, Egypt
[f] Faculty of Computer Science and Engineering, Galala University, Suze, 435611, Egypt
[g] Department of Computer Science, College of Computer and Information Sciences, King Saud University, Riyadh 11633, Saudi Arabia
[h] School of Computer Science and Electronic Engineering, University of Essex, Colchester, UK

ARTICLE INFO

Keywords:
Beamspace processing
Compressive sensing
Direction of arrival estimation
Fluctuating sources
Nested array

ABSTRACT

In the pursuit of enabling the unprecedented capabilities of the sixth-generation (6G) technology, this paper endeavours to advance the state-of-the-art in the direction of arrival (DOA) estimation techniques for dynamic scenarios. This work introduces an innovative adaptive compressive sensing (CS) technique, termed the BS weighted-CSKF algorithm. This approach integrates CS principles with a CS-oriented Kalman filter (KF), providing enhanced adaptability to fluctuating and moving source signals. Comparative analysis against existing CS-based DOA estimation methods demonstrates the superior performance of the proposed algorithm, particularly in low signal-to-noise ratio (SNR) environments. Notably, the BS weighted-CSKF algorithm operates effectively even in unknown noise field scenarios, eliminating the requirement for orthogonality between the signal and subspace noise or singular value decomposition. This capability enables accurate DOA estimation without prior knowledge of the number of signal sources. Additionally, investigations into rank-one updates of the covariance matrix highlight the algorithm's ability to estimate a higher number of sources than sensors employed without imposing constraints on source properties. The algorithm's versatility extends to coherent and spatially correlated sources, further enhancing its applicability in diverse scenarios. Moreover, employing BS CS-based DOA estimation techniques yields a significant computational load reduction, exceeding 35% compared to the conventional element-space (ES) CS-based approach. Leveraging the proposed technique, fluctuating moving source signals can be efficiently detected and tracked using fewer snapshots, facilitating real-time monitoring and analysis in dynamic environments.

* Corresponding author.
E-mail addresses: amgad.salama@acm.org (A.A. Salama), mahmoud.shawky@glasgow.ac.uk (M.A. Shawky), salord1960@yahoo.com (S.H. Darwish), adhamegypt0@gmail.com (A.A. Elmahallawy), abd_el_aziz_m@yahoo.com (M.A. Elaziz), Ahalmogren@ksu.edu.sa (A. Almogren), ag.abdellatef@zu.edu.eg (A.G. Abdellatif), syed.shah@essex.ac.uk (S.T. Shah).

https://doi.org/10.1016/j.iot.2024.101486
Received 21 October 2024; Received in revised form 9 December 2024; Accepted 22 December 2024
Available online 30 December 2024

1. Introduction

The internet-of-things (IoT) has revolutionised interactions with the surrounding environment, from smart homes to advanced industrial systems, by introducing a network of interconnected devices. Central to many IoT applications is the need for precise localisation and tracking of devices, a task where direction of arrival (DOA) estimation plays a pivotal role. In environments such as smart buildings and factories, accurate DOA estimation is critical for optimising operations. For instance, in a smart factory, real-time tracking of sensors and autonomous robots ensures synchronised workflows, enhancing both efficiency and safety. Similarly, in emergency scenarios, pinpointing the location of IoT devices can be lifesaving, especially in areas where conventional positioning systems are ineffective [1–3].

The rising integration of aerial IoT platforms, such as unmanned aerial vehicles (UAVs), introduces additional complexities, including maintaining reliable connectivity and mitigating interference in dynamic conditions. Super-resolution DOA estimation is achievable through subspace approaches like MUSIC [4] and ESPRIT [5]. However, these methods require a high signal-to-noise ratio (SNR) and sufficient snapshots to perform accurately. To address limitations in challenging conditions, several sparse signal recovery (SSR) techniques for DOA estimation have been developed [6–11]. These techniques have been shown to outperform subspace methods in scenarios with few snapshots, low SNR, and closely spaced signals by leveraging SSR theory and the sparsity of the spatial domain. The primary SSR-based DOA estimation approaches can be categorised into four main types: matching pursuit (MP) [12,13], ℓ_p-norm-based methods [14], covariance-based methods [15], and sparse Bayesian learning (SBL) methods [16,17].

The lack of super-resolution in MP techniques is attributed to the problem of error propagation [18]. In contrast, ℓ_p-norm methods transform the DOA estimation into a convex optimisation problem, yielding more precise estimates than those obtained by MP approaches. However, the effectiveness of ℓ_p-norm-based approaches depends on the penalty operation, and determining the regularised values can be challenging [19]. Covariance-based methods, unlike ℓ_p-norm methods, do not require difficult parameter selection and can perform DOA estimation without predetermined grids [20]. Nonetheless, these methods necessitate solving semidefinite programming problems, which involve high computational complexity. SBL techniques address the signal recovery problem by constructing a probabilistic Bayesian framework with sparse priors [21] and iteratively updating the hyperparameters. These techniques avoid the need to select regularised parameters by learning the hyperparameters from the data. Despite this advantage, SBL methods still face challenges in real-world applications due to their significant computational complexity [22].

To increase the sensor array aperture virtually and enhance array performance, sparse arrays have been introduced [23]. A virtual sensor array is a technique that enables DOA estimation using a simulated array of sensors rather than a physical one. This approach is particularly effective in scenarios where deploying a physical sensor array is not feasible or is prohibitively expensive. Instead of relying on an actual array of sensors, a virtual sensor array employs algorithms to replicate the behaviour of an array using data from a limited number of sensors. This technique exploits the spatiotemporal properties of signals, making it possible to estimate the DOA effectively. The adoption of virtual sensor arrays has significantly expanded the capabilities of DOA estimation, proving to be a valuable tool in signal-processing applications where spatial localisation is critical [24–30].

Source signal tracking is a signal processing technique that involves the real-time localisation and tracking of a source signal, as shown in Fig. 1. The primary goal is to compute the source signal's direction of arrival (DOA) and continuously track this DOA as the signal moves. This information is crucial for locating the source and identifying any changes in the signal. Source signal tracking is an essential tool in various fields, including acoustic signal processing, radar systems, and wireless communications. A two-step semi-supervised learning-based range estimation approach for source signal tracking is proposed in [31]. Additionally, an adaptive grid refinement (AGR) sparse Bayesian learning (SBL) method has been developed to enhance efficiency and performance when using coarse initial grid points [32]. Furthermore, a trajectory-oriented Poisson Multi-Bernoulli mixture approach has been introduced for matched field tracking, ensuring trajectory continuity of the flickering target and correcting localisation defects in matched field processing [33].

It should be noted that most of the aforementioned tracking techniques are learning-based and rely heavily on a substantial amount of labelled data to achieve acceptable performance. This reliance not only limits their adaptability to dynamic environments but also increases the computational complexity, rendering these methods unsuitable for real-time applications. Additionally, these techniques are predominantly developed using element-space data, which further compounds their computational burden, particularly in scenarios involving high-density IoT deployments. Addressing these challenges, this paper proposes a novel technique for DOA estimation using a sparse linear array in the beamspace (BS). By leveraging the beamspace domain, the computational efficiency of the proposed method is significantly enhanced, making it suitable for real-time operations in dynamic and interference-prone environments.

The core contribution of this study lies in introducing an adaptive beamspace compressed sensing (BS CS)-based DOA estimation technique, capable of handling fluctuating and moving source signals. The proposed method enables the estimation and tracking of a greater number of source signals than the physical sensors present in the array, a critical advancement for dense IoT networks and next-generation 6G applications. Additionally, the algorithm's spatial filtering capabilities effectively mitigate interference, ensuring optimal performance in crowded environments. Notably, the technique achieves a 35% reduction in computational load compared to traditional methods, extending IoT device battery life and promoting sustainable network operations. These advancements position the proposed method as a robust and scalable solution, with transformative implications for diverse applications such as smart cities, healthcare, and agriculture, bridging the gap between theoretical innovation and practical deployment. The significant contributions of this work are as follows:

1. *Latency reduction*: To minimise latency, the proposed algorithm applies a rank-one update of the covariance matrix, making it a single snapshot method.

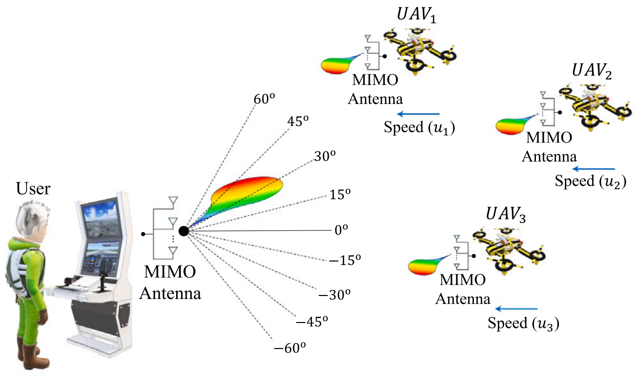

Fig. 1. The system architecture of the proposed DOA estimation technique for flying ad-hoc networks (FANET).

2. *Computational efficiency*: The DOA estimation problem is reformulated in the BS domain with calculations transformed into real numbers, significantly reducing the computational load.
3. *Enhanced tracking*: The tracking task is carried out by a Kalman filter utilising the real data obtained through BS transformation. The Kalman filter's subprocesses—prediction, measurement update, and output—are all reformulated in the CS domain to ensure effective DOA estimation.
4. *Realistic signal handling*: The proposed technique is tested with multiple fluctuating source signals, various moving scenarios, and different BS methods, contrasting with other works that only consider constant amplitude signals. This ensures the method's effectiveness in practical environments.

Furthermore, the proposed DOA estimation method, operating at the physical layer, processes RF signals independently of higher-layer protocols, ensuring flexibility and seamless integration into diverse network architectures. By directly interfacing with the physical layer and transmitting estimated DOA information to higher layers via standard interfaces, this modular design enables effortless incorporation into existing IoT and 6G infrastructures without significant protocol modifications. Additionally, it maintains real-time processing capabilities, ensuring robust performance in dynamic, resource-constrained environments.

The rest of this paper is structured into four main sections. Section 2 provides a brief introduction to element-space compressed sensing (CS)-based direction of arrival (DOA) estimation. In Section 3, we introduce the novel adaptive BS CS Kalman filter (CSKF). The performance evaluation of our method is conducted through simulations in Section 4. Finally, conclusions are given in Section 5.

Note: The superscript $\{\}^H$ denotes the conjugate transpose operation, while $\{\}^*$ represents conjugation without transpose, and $\{\}^T$ signifies the transpose operation. Additionally, the symbol $\odot$ indicates the Khatri–Rao (KR) product [34] between two matrices of appropriate dimensions.

2. Compressive sensing framework

Given that the source signals are far-field sources, they can be treated as point sources, which leads to sparsity in space. Leveraging this sparsity property from a CS perspective, the mathematical representation of the sensor array output, $\mathbf{y} \in \mathbb{C}^{M\times 1}$, is as follows.

$$\mathbf{y}(t) = \boldsymbol{\Phi}\mathbf{s}(t) + \mathbf{n}(t) \tag{1}$$

where $\boldsymbol{\Phi} \in \mathbb{C}^{M\times N}$ represents the over-complete steering matrix, denoted by

$$\begin{aligned}\boldsymbol{\Phi} &= [\mathbf{a}(\theta_1)\ \mathbf{a}(\theta_2)\ \dots\ \mathbf{a}(\theta_n)\ \dots\ \mathbf{a}(\theta_N)] \\ &= \begin{bmatrix} e^{jk_o d(-(M-1)/2)\cos\theta_1} & \dots & e^{jk_o d(-(M-1)/2)\cos\theta_N} \\ \vdots & & \vdots \\ 1 & \ddots & 1 \\ \vdots & & \vdots \\ e^{jk_o d((M-1)/2)\cos\theta_1} & \dots & e^{jk_o d((M-1)/2)\cos\theta_N} \end{bmatrix}\end{aligned} \tag{2}$$

and $\mathbf{n} \in \mathbb{C}^{M\times 1}$ is the additive white Gaussian noise (AWGN). Here, $\mathbf{a}(\theta_n) \in \mathbb{C}^{M\times 1}$ denotes the steering vector of the virtual array associated with the angle of arrival (AOA) of (θ_n). In (2), $\{\theta_n\}_{n=1}^{N}$ indicates a grid covering the set of all conceivable positions, Ω and $N \gg L$. Therefore, the vector of source signal $\mathbf{s} \in \mathbb{C}^{N\times 1}$ is provided by

$$\mathbf{s}(t) = [\sigma_1\ \sigma_2\ \dots\ \sigma_n\ \dots\ \sigma_N]^T \tag{3}$$

where the nth element of $\mathbf{s}(t)$, $s_n(t)$, is non-zero only if $(\theta_n = \theta_l)$ where $1 \geq l \geq L$ is the source signal number and, in that case, $\sigma_n = \sigma_l$. In the case of CS, the concern lies in the estimation of $\mathbf{s}$ given the sensor array output, $\mathbf{y}$. In a noise-free scenario, sparsity in $\mathbf{s}$ can be investigated by minimising the ℓ_0-norm, which determines the number of non-zero elements in the vector $\mathbf{s}$. This is formulated as:

$$\min_{\mathbf{s}} \|\mathbf{s}\|_0 \text{ subject to } \mathbf{y} = \boldsymbol{\Phi}\mathbf{s} \tag{4}$$

However, it is known that reducing this problem is NP-hard [35], making it computationally intractable even for problems of moderate dimensions. Consequently, CS has explored various methods to approximately solve the ℓ_0-norm problem [35–38]. It has been demonstrated that for sensing matrices with sufficiently incoherent columns and sufficiently sparse signals, [39,40], the ℓ_0-norm problem is equivalent to the ℓ_1-norm one [41–43] where ℓ_1 minimisation is determined as

$$\min_{\mathbf{s}} \|\mathbf{s}\|_1 \text{ subject to } \mathbf{y} = \boldsymbol{\Phi}\mathbf{s} \tag{5}$$

Furthermore, the ℓ_2-norm could be employed as an alternative strategy to address the ℓ_0-norm problem by relaxing the ℓ_0-norm into the ℓ_2-norm. This is expressed as:

$$\min_{\mathbf{s}} \|\mathbf{s}\|_2 \text{ contingent upon } \mathbf{y} = \boldsymbol{\Phi}\mathbf{s} \tag{6}$$

Being convex in nature, this problem can be analytically resolved by

$$\hat{\mathbf{s}} = \boldsymbol{\Phi}^H(\boldsymbol{\Phi}\boldsymbol{\Phi}^H)^{-1}\mathbf{y} \tag{7}$$

However, the ℓ_1-norm problem tends to favour sparse signals more than the ℓ_2-norm. Additionally, the relaxation of the ℓ_1-norm is a convex optimisation that converges to the global minimum and is most similar to the ℓ_0-norm [44].

In practical applications, CS can be extended to accommodate scenarios involving measurements corrupted by noise. The formulation of the ℓ_1-norm problem for noisy measurements can be presented as follows.

$$\min_{\mathbf{s}} \|\mathbf{s}\|_1 \text{ subject to } \|\boldsymbol{\Phi}\mathbf{s} - \mathbf{y}\|_2 \le \beta \tag{8}$$

where β represents the tolerance error ($\beta > 0$). The ℓ_2-norm is utilised for error evaluation $\boldsymbol{\Phi}\mathbf{s} - \mathbf{y}$, although it can be substituted with any other norm, such as ℓ_∞ or ℓ_p, $0 < p \ge 1$. The selection of β is assumed to be related to the residuals of the solution, known as the discrepancy principle [45,46]. An ℓ_1-norm constrained form of Eq. (8) is commonly known as the least absolute shrinkage and selection operator (LASSO) [47]. The LASSO minimisation problem can be formulated as:

$$\min_{\mathbf{s}} \|\mathbf{y} - \boldsymbol{\Phi}\mathbf{s}\|_2^2 + \tau\,\|\mathbf{s}\|_1 \tag{9}$$

In the context of regularisation, the parameter τ is a non-negative value used for regularisation. The ℓ_1 penalisation strategy is also known as *basis pursuit* [48]. A modified version of LASSO called minimum variance distortionless response adaptable LASSO (MVDR A-LASSO) is proposed in [10]. The study demonstrated that MVDR A-LASSO outperforms both traditional DOA estimation techniques and LASSO-based DOA estimation, as described in [10].

$$\hat{\mathbf{s}}^{(k)} = \min_{\mathbf{s}} \|\mathbf{y} - \boldsymbol{\Phi}\mathbf{s}\|_2^2 + \tau_k \sum_{n=1}^{N} \hat{\omega}_n |s_n| \tag{10}$$

where k represents the iteration number, $\hat{\omega}_n$ denotes the nth element of the weight vector, and $\hat{\mathbf{w}}$ and $\hat{\mathbf{w}}$ is obtained by MVDR at $k = 1$.

3. Adaptive weighted-CSKF

By understanding the system dynamics and the measurement device, along with statistical insights into system noises, measurement errors, uncertainties in dynamic models, and initial conditions of variables, the Kalman filter (KF) facilitates the estimation of the present value of the desired variable. The KF is an optimal recursive data processing technique that effectively integrates all available information to generate estimates of desired variables while minimising statistical errors. From a Bayesian perspective, the KF advances the conditional probability density of the desired quantities by incorporating information obtained from observed measurement data. It is important to note that the system is assumed to be described by a linear model, with all noises and errors considered white and characterised as Gaussian processes [49].

Assume a random discrete-time process $\left\{\mathbf{g}_k \in \mathbb{R}^N\right\}_{k=1}^{\infty}$ that is sparse in some known orthonormal sparsity basis $\psi \in \mathbb{R}^{N\times N}$, that is $\mathbf{s}_k = \psi^T\mathbf{g}_k$, $\#\{\text{supp}(\mathbf{s}_k)\} < N$, where $\text{supp}(\mathbf{s}_k)$ denotes the support of $\mathbf{s}_k$ and $\#\{\text{supp}(\mathbf{s}_k)\}$ is the number of non-zero elements of $\mathbf{s}_k$. Consider $\mathbf{s}_k$ is evolving as

$$\mathbf{s}_{k+1} = \mathbf{A}\mathbf{s}_k + \mathbf{w}_k, \quad \mathbf{s}_0 \sim \mathcal{N}(\mu_0, P_0) \tag{11}$$

where $\mathbf{A} \in \mathbb{R}^{N\times N}$ is the state transition matrix and $\{\mathbf{w}_k\}_{k=1}^{\infty}$ is a zero-mean white Gaussian process with covariance $\mathbf{Q}_k \ge 0$. The process $\mathbf{y}_k$ is measured by

$$\mathbf{y}_k = \mathbf{H}\mathbf{g}_k + \mathbf{n}_k = \boldsymbol{\Phi}\mathbf{s}_k + \mathbf{n}_k \tag{12}$$

where $\mathbf{H} := \boldsymbol{\Phi}\psi^T \in \mathbb{R}^{M\times N}$. In order to estimate $\hat{\mathbf{s}}$ using the system defined by (11) and (12), KF can be expressed as

$$\min_{\hat{\mathbf{s}}_k} E_{\mathbf{z}_k|\mathbf{y}^k}\left[\left\|\mathbf{z}_k - \hat{\mathbf{z}}_k\right\|_2^2\right] \tag{13}$$

which can be reformulated as

$$\min_{\hat{\mathbf{s}}_k} E_{\mathbf{z}_k|\mathbf{y}^k}\left[\left\|\mathbf{z}_k-\hat{\mathbf{z}}_k\right\|_2^2\right] \text{ subject to } \left\|\hat{\mathbf{z}}_k\right\|_1 \leq \tau' \tag{14}$$

Eq. (14) can be solved using the classical KF framework. Yet, since our CS problem is ill-posed, as illustrated in Section 4, applying an ordinary KF is useless. However, it can be solved using the pseudo-measurement (PM) technique [50]. $\left\|\hat{\mathbf{z}}_k\right\|_1 \leq \tau'$ can be adopted for ill-posed problems using PM technique by introducing a dummy measurement $0=\left\|\hat{\mathbf{z}}_k\right\|_1-\tau'$, which can be rewritten as follow [51].

$$0=\bar{\Phi}\mathbf{z}_k-\tau', \quad \bar{\Phi}:=\left[\operatorname{sign}(z_k(1)),\ldots,\operatorname{sign}(z_k(N))\right] \tag{15}$$

where $\operatorname{sign}(z_k(n)),\ n=\{1,\ldots,N\}$ denotes the sign function of the nth element of $\mathbf{z}_k$ where

$$\operatorname{sign}(z_k(n))=\begin{cases}1 & \text{if } z_k(n)\geq 0\\ -1 & \text{otherwise}\end{cases} \tag{16}$$

Building upon the framework established by A-LASSO [10], we propose a novel approach for the DOA estimation termed "adaptive weighted-CSKF". This variant of CSKF allows for adaptability through the adjustment of initial weights, in alignment with the methodology outlined in A-LASSO [10]. Algorithm 1 illustrates the implementation of the adaptive weighted CSKF in a single iteration. Notably, the adaptive weighted CSKF is utilised within the context of the CS, as follows.

$$\Phi'=\Phi^*, \quad \mathbf{y}_k=\mathbf{y}_{es} \tag{17}$$

where Φ' represents a modified version of the matrix Φ, and it is equivalent to the conjugate transpose of Φ, denoted as Φ^*. In addition, y_k is equal to y_{es}, suggesting that the measurement vector y_k at time step k is identical to the expected (or estimated) measurement vector y_{es}. In the adaptive weighted-CSKF simulations, a multi-beam beamspace approach is employed, where the number of beams in the fan beam for each source, denoted as N_{bs}, is set to 3. Following each iteration of the adaptive weighted-CSKF, the beamspace projection matrix $\mathbf{B}^H_{bs,total}$ is updated using the estimated DOA of the source signals, with each estimated angle of arrival (AOA) serving as the centre beam, θ_c, of the fan beams. Fig. 2 outlines the steps involved in the proposed adaptive weighted-CSKF method. Consequently, the estimated signal $\hat{\mathbf{s}}$ is utilised to compute the new weight vector $\mathbf{w}$ for the subsequent iteration of the adaptive weighted-CSKF algorithm.

Algorithm 1 The adaptive weighted-CSKF

1: *Initialisation*
Let the initial estimate for s be $\hat{s}$.
Find $\hat{\mathbf{w}}$, where the n-th element of $\hat{\mathbf{w}}$, $\hat{w}_n$, is given by $\hat{w}_n=1/\left|\hat{s}_n\right|^\gamma, \quad n=1,\ldots,N$.
Define $\Phi\in\mathbb{C}^{M\times N}$ matrix, such that its (m,n)-th element is given by $\phi_{mn}/\hat{w}_n$, where $m=1,\ldots,M$ and $n=1,\ldots,N$.

2: *Beamspace transformation*

$$\Phi'=\mathbf{B}^H_{bs}\Phi \quad (\Phi'\in\mathbb{R}^{N_{bs}\times N}) \tag{18a}$$

$$\mathbf{y}_k=\mathbf{y}_{bs}=\mathbf{B}^H_{bs}\mathbf{y}_{es} \quad (\mathbf{y}_{bs}\in\mathbb{R}^{N_{bs}\times 1}) \tag{18b}$$

3: *Prediction*

$$\hat{\mathbf{s}}_{k+1|k}=\mathbf{A}\hat{\mathbf{s}}_{k|k} \tag{19a}$$

$$\mathbf{P}_{k+1|k}=\mathbf{A}\mathbf{P}_{k|k}\mathbf{A}^T+\mathbf{Q}_k \tag{19b}$$

4: *Measurement Update*

$$\mathbf{K}_k=\mathbf{P}_{k+1|k}\Phi'^T\left(\Phi'\mathbf{P}_{k+1|k}\Phi'^T+\mathbf{R}_k\right)^{-1} \tag{20a}$$

$$\hat{\mathbf{s}}_{k+1|k+1}=\hat{\mathbf{s}}_{k+1|k}+\mathbf{K}_k\left(\mathbf{y}_k-\Phi'\hat{\mathbf{s}}_{k+1|k}\right) \tag{20b}$$

$$\mathbf{P}_{k+1|k+1}=\left(\mathbf{I}-\mathbf{K}_k\Phi'\right)\mathbf{P}_{k+1|k} \tag{20c}$$

5: *CS Pseudo Measurement:* Let $\mathbf{P}^1=\mathbf{P}_{k+1|k+1}$ and $\hat{\mathbf{s}}^1=\hat{\mathbf{s}}_{k+1|k+1}$

6: **for** $\zeta=1,2,\ldots,N_\zeta-1$ iterations **do**

$$\bar{\Phi}_\zeta=\left[\operatorname{sign}(\hat{s}^\zeta(1)),\ldots,\operatorname{sign}(\hat{s}^\zeta(n))\right] \tag{21a}$$

$$\mathbf{K}^\zeta=\mathbf{P}^\zeta\bar{\Phi}_\zeta^T\left(\bar{\Phi}_\zeta\mathbf{P}^\zeta\bar{\Phi}_\zeta^T+R_\epsilon\right)^{-1} \tag{21b}$$

$$\hat{\mathbf{s}}^{\zeta+1}=\left(\mathbf{I}-\mathbf{K}^\zeta\bar{\Phi}_\zeta\right)\hat{\mathbf{s}}^\zeta \tag{21c}$$

$$\mathbf{P}^{\zeta+1}=\left(\mathbf{I}-\mathbf{K}^\zeta\bar{\Phi}_\zeta\right)\mathbf{P}^\zeta \tag{21d}$$

7: **end for**
8: Calculate $\hat{\mathbf{s}}^{N_\zeta}=\hat{s}_n^{N_\zeta}/\hat{w}_n, \quad n=1,\ldots,N$
9: Set $\mathbf{P}_{k+1|k+1}=\mathbf{P}^{N_\zeta}$ and $\hat{\mathbf{s}}_{k+1|k+1}=\hat{\mathbf{s}}^{N_\zeta}$

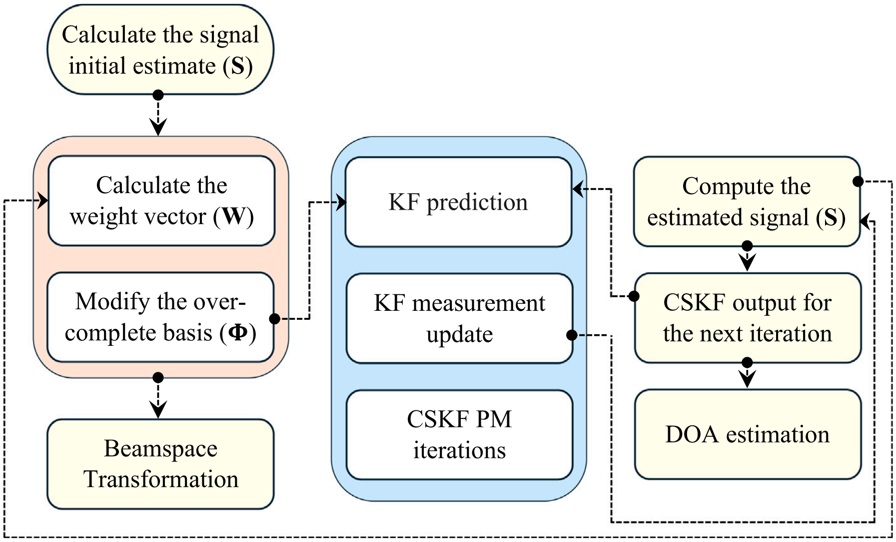

Fig. 2. Block diagram of the weighted-CSKF for estimating the DOA of moving signal sources.

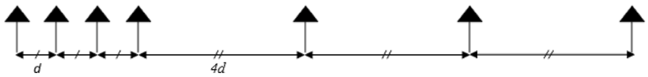

Fig. 3. An array with two levels of nesting, containing 7 elements.

The algorithm begins with an initialisation step, where the initial estimate for the signal $\hat{s}$ is computed based on available information. Subsequently, the algorithm performs a beamspace transformation, converting the measurement vector $\mathbf{y}_k$ into a beamspace representation $\mathbf{y}_{bs}$. Next, the algorithm predicts the state of the system using the Kalman filter prediction equations, updating the state estimate $\hat{\mathbf{s}}$ and the error covariance matrix $\mathbf{P}$. Following the prediction step, a measurement update is performed, incorporating the observed measurements and refining the state estimate based on Kalman filter measurement update equations. Additionally, the algorithm employs a compressed sensing pseudo-measurement (CS PM) technique to address the ill-posed nature of the compressive sensing problem, iteratively refining the estimates through multiple iterations. Finally, the algorithm concludes by calculating the final state estimate $\hat{\mathbf{s}}_{k+1|k+1}$ and error covariance matrix $\mathbf{P}_{k+1|k+1}$ for the next time step, completing the iteration process. Overall, the algorithm integrates the principles of compressed sensing and Kalman filtering to iteratively estimate the state of the system, demonstrating adaptability and robustness in the face of sparse signals and noisy measurements. Note that the Cramer–Rao lower bound (CRLB) for the proposed algorithm, namely the adaptive weighted-CSKF, is derived in Appendix A.1.

4. Simulation results

Consider a sparse linear, two-level nested array comprising M elements, where M is odd. This array is structured with 3 elements in the first level and 4 elements in the second level, as depicted in Fig. 3. Upon analysing the array and isolating the unique virtual elements from the virtual array manifold ($\mathbf{A}^* \odot \mathbf{A}$), it becomes evident that the virtual array forms a uniform linear array consisting of $M = 31$ elements. The sampling grid $\theta_n \in [1^\circ : 180^\circ]$, covering Ω, is selected with a 1° step size. The signal sources are modelled as $e^{j2\pi f_d t}$, where f_d represents the Doppler frequency. Furthermore, it is assumed in the simulation that the source signals are heading towards the array. For both fixed and moving source signals, 10 snapshots are assumed for the initial covariance matrix calculation, denoted as $\hat{R}_{xx}$. This is followed by the rank-one update of Eq. (20).

For beamspace processing [11], in multiple-beam beamspace (MBS) simulations, the number of beams, denoted as N_{bs}, is set to $N_{bs} = 1$ for each source signal in fixed source signal simulations, whereas $N_{bs} = 3$ is used for scenarios involving moving source signals. In all simulations, except for the last three, a single iteration of MVDR A-LASSO [10] is utilised. Furthermore, during the simulations, it is with each other and the noise, except in the third simulation where the sources are intentionally correlated. The value of ϵ, is set to 0.1 in all the simulations except for the first simulation. In addition, the total number of trials, N_{sim}, is set to $N_{sim} = 100$ for each observation point. For each experiment, the regularisation parameter, τ, is selected based on the idea of the L-curve [52,53] and by using the identical method outlined in [10].

The performance evaluation of the proposed beamspace algorithms is conducted using the CVX toolbox [54,55], a software package designed for convex optimisation that seamlessly integrates with the MATLAB environment. To obtain the global solution

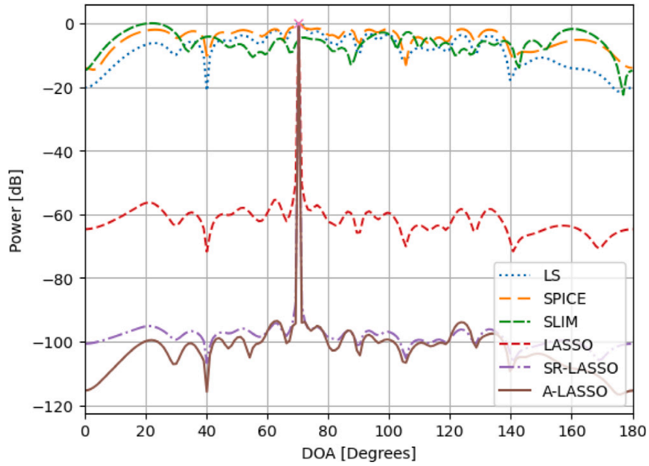

Fig. 4. LS, SPICE, SLIM, LASSO, SR-LASSO, and A-LASSO performance for source signal at DOA of 70°, SNR = 10 dB and one iteration.

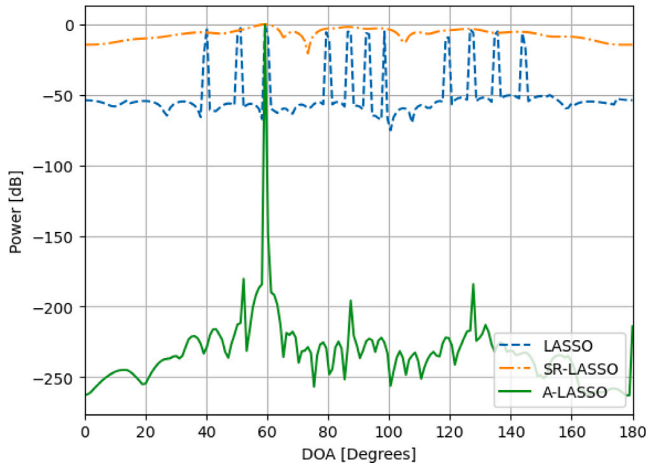

Fig. 5. LASSO, SR-LASSO, and A-LASSO performance for source signal at DOA of 60°, SNR = −10 dB and five iterations.

for the optimisation problem, the CVX toolbox utilises semi-definite quadratic–linear programming (SDPT3) [56]. The root mean square error (RMSE) is employed as the performance metric, formulated as

$$RMSE = \frac{1}{L}\sum_{l=1}^{L}\sqrt{\frac{1}{N_{sim}}\sum_{n=1}^{N_{sim}}(\hat{\theta}_{l,n}-\theta_l)^2} \tag{22}$$

where $\hat{\theta}_{l,n}$ is the estimate of the DOA angle θ_l of the nth Monte Carlo trial.

4.1. Investigation of the proposed algorithm with various CS-based DOA estimation

In the initial simulation, the performance of the proposed method is compared with several other algorithms, including least squares (LS), sparse iterative covariance-based estimation (SPICE) [57,58], sparse learning via iterative minimisation (SLIM) [59], LASSO [47], square-root LASSO (SR-LASSO) [58], and A-LASSO [10]. The array configuration utilised in the simulation, depicted in Fig. 3, comprises seven elements. The scenario involves a source signal arriving at the sparse array from a DOA of 70°. The results, presented in Fig. 4, illustrate the performance of these algorithms under a high signal-to-noise ratio (SNR) of 10 dB with a single iteration. Notably, A-LASSO, SR-LASSO, and LASSO outperform LS, SPICE, and SLIM even at high SNR levels. Additionally, it is observed that increasing the number of iterations enables A-LASSO to achieve superior performance compared to both SR-LASSO and LASSO.

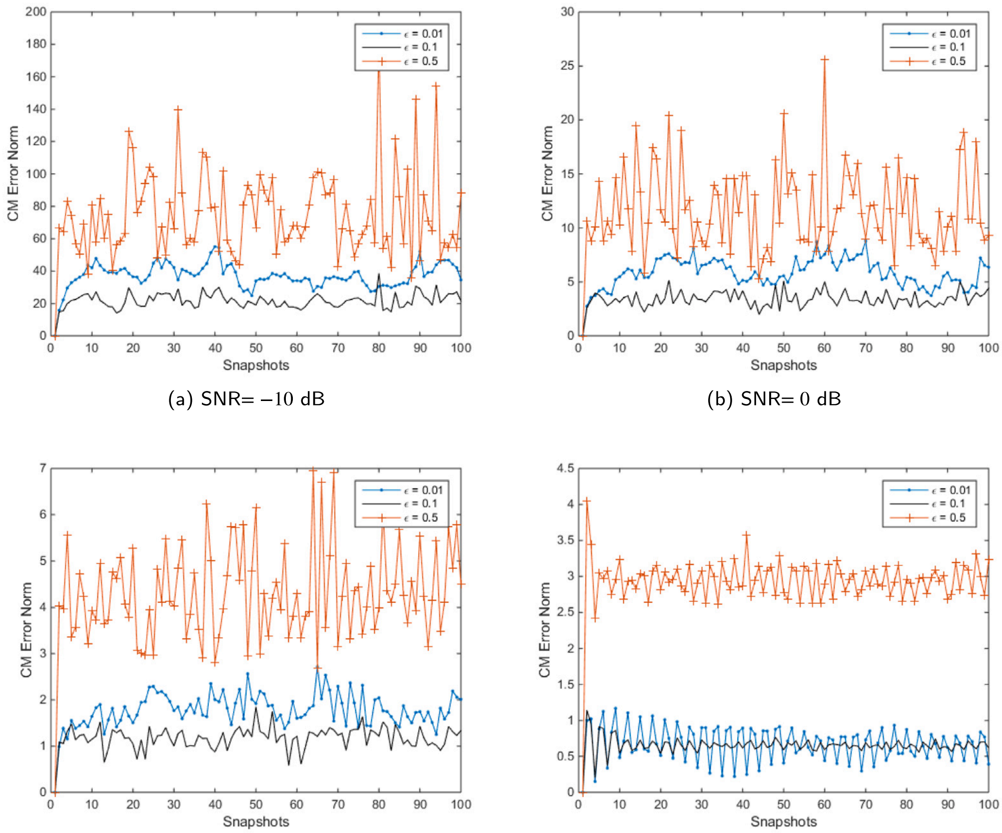

(a) SNR= −10 dB (b) SNR= 0 dB

(c) SNR= 10 dB (d) SNR= 30 dB

Fig. 6. The rank-one updated covariance matrix error for different values of ϵ. SNR = (a) −10 dB, (b) 0 dB, (c) 10 dB, and (d) 30 dB.

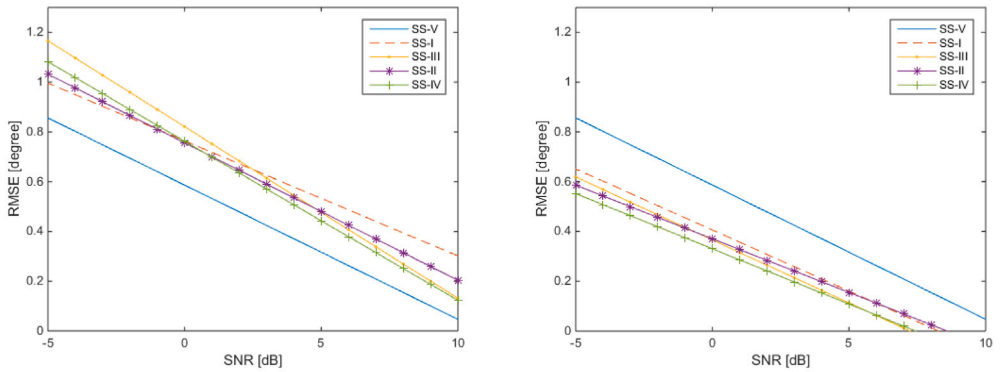

(a) $N_{in} = 0$ (b) $N_{in} = 50$

Fig. 7. Performance of the two source signals for the ES CS-based DOA estimate when the SNR is changed at DOAs of 60° and 120°, N_{in} = 0 and 50, using different Swerling source signals.

In the second simulation, the performance of the proposed A-LASSO algorithm, along with LASSO and SR-LASSO algorithms, is evaluated under more realistic conditions, with a SNR reduced to −10 dB. In this scenario, the source signal impinges on the sparse array from a DOA of 60°. Results obtained with a SNR of −10 dB and five iterations of A-LASSO are depicted in Fig. 5, illustrating the superior performance of A-LASSO. Conversely, both the SR-LASSO and LASSO methods fail to accurately estimate the DOA, with the LASSO-based approach exhibiting sparsity leakage and false source signals, leading to the fusion of source signals. These findings highlight the limitations of using LASSO or SR-LASSO algorithms in such scenarios.

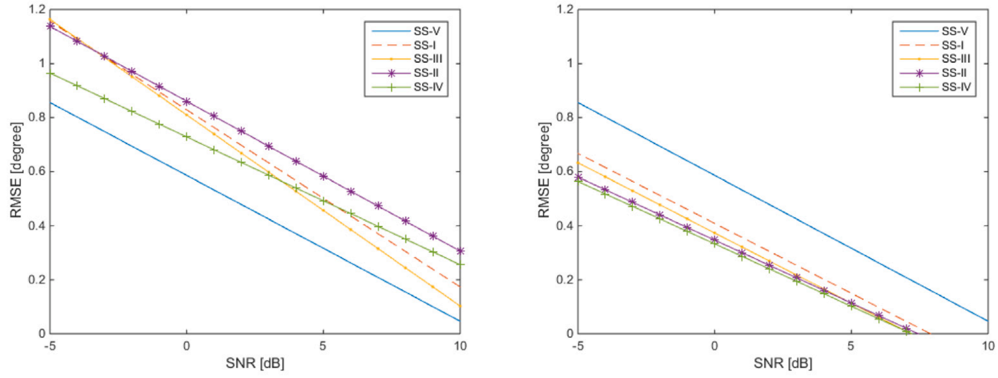

(a) $N_{in} = 0$ (b) $N_{in} = 50$

Fig. 8. Performance of full-dimension beamspace CS-based DOA estimate for two source signals when SNR is changed at DOAs of 60° and 120°, $N_{in} = 0$ and 50, utilising various Swerling source signals.

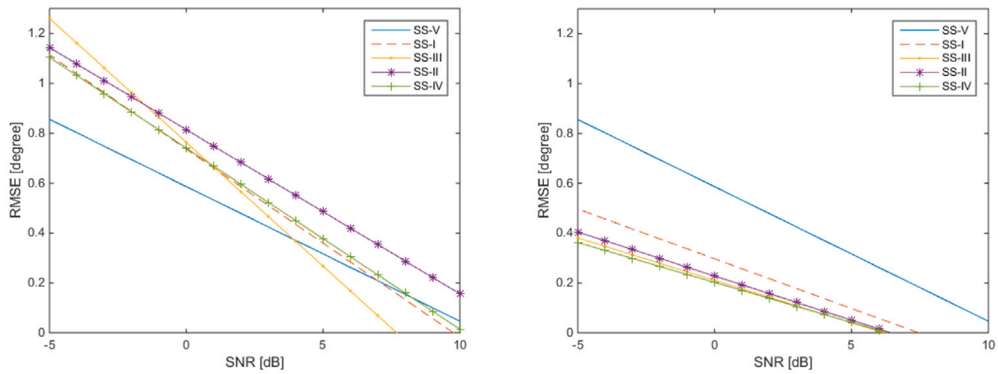

(a) $N_{in} = 0$ (b) $N_{in} = 50$

Fig. 9. Performance of MBS CS-based DOA estimate for two source signals when SNR is changed at DOAs of 60° and 120°, $N_{in} = 0$ and 50, utilising various Swerling source signals.

4.2. Investigation of the rank-one updated covariance matrix

The third simulation focuses on analysing the rank-one update of the covariance matrix, as described in (20), for real-time updates of the estimated covariance matrix, $\hat{\mathbf{R}}_{xx}$. Fig. 6 illustrates the covariance matrix error norm, $\|\hat{\mathbf{R}}_{xx(normal)} - \hat{\mathbf{R}}_{xx(20)}\|_2$, as $\hat{\mathbf{R}}_{xx}$ is updated using new incoming snapshots for different values of ϵ (subscripts denote the equation used to calculate $\hat{\mathbf{R}}_{xx}$). With 100 snapshots, $\epsilon = 0.01, 0.1$, and 0.5, and SNRs of −10, 0, 10, and 30 dB, the covariance matrix error is depicted. It is observed that increasing the SNR minimises the covariance matrix error for all values of ϵ. For low and moderate SNRs, $\epsilon = 0.1$ results in the minimum error compared to $\epsilon = 0.01$ and $\epsilon = 0.5$. Furthermore, at high SNRs, Fig. 6 indicates that the error corresponding to $\epsilon = 0.1$ is more stable and saturates compared to that of $\epsilon = 0.01$, while the error using $\epsilon = 0.5$ is considerably higher. Considering the results of the first simulation, ϵ was set to 0.1 for all subsequent simulations.

4.3. Investigation of fluctuating source signals

In the following simulations, we explore the impact of various Swerling source signals. In the fourth simulation, we assess the performance of ES CS-based DOA estimation while varying the SNR. The nested array is subjected to two source signals arriving from DOA angles of 60° and 120°, respectively. The SNR is changed across a range from −5 dB to 10 dB. Additionally, in line with conventional approaches for addressing Swerling source signal detection, we aggregate the outputs of the virtual array, where the number of integrated snapshots, N_{in}, is set to be 0 and 50. Four different Swerling source signals are assumed. Element-space DOA estimation error for the figures includes Swerling-V as a reference where N_{in} is set to 0 in this case. The performance of the ES CS-based DOA estimation algorithm is illustrated in Fig. 7. From this figure, it is evident that augmenting the number of integrated snapshots, N_{in}, leads to better DOA estimation, where increasing N_{in} to be 50 snapshots reduced the DOA estimation error by almost 50% for all Swerling source signals for low SNR.

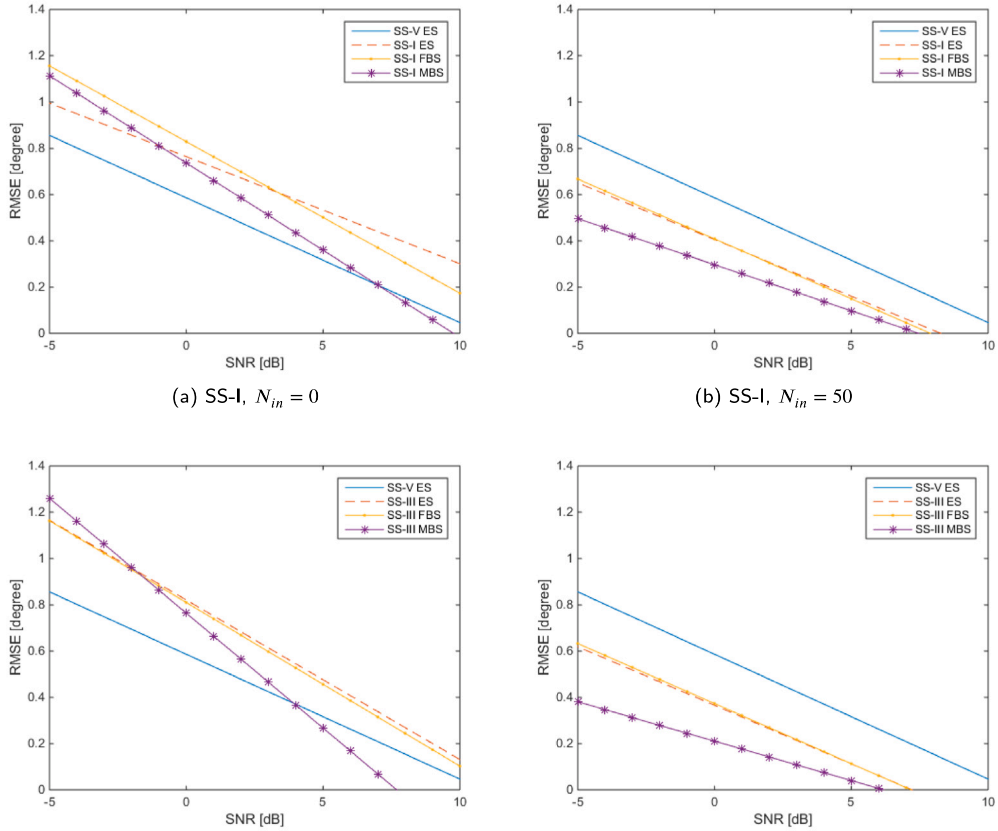

(a) SS-I, $N_{in} = 0$ (b) SS-I, $N_{in} = 50$

(c) SS-III, $N_{in} = 0$ (d) SS-III, $N_{in} = 50$

Fig. 10. Performance of CS-based DOA estimate for two source signals when SNR is changed at DOAs of 60° and 120°, N_{in} = 0 and 50, Swerling-I and -III source signals, using ES, FBS, and MBS.

We investigate the performance of full-dimension beamspace CS-based DOA estimation across varying SNRs in the fifth simulation. Following the methodology employed in the fourth simulation, a fully-dimensioned beamspace (FBS) configuration with 31 beams is utilised. The study encompasses four potential Swerling source signals. Figures portray the element-space DOA estimate error for Swerling-V as a reference, with N_{in} set to 0 in this context. The efficacy of the FBS CS-based DOA estimation algorithm is elucidated in Fig. 8, highlighting that augmenting N_{in} to 50 snapshots reduces the DOA estimation error by approximately 50% compared to $N_{in} = 0$. Particularly noteworthy is the observation, evident from Fig. 8(a), that at low SNRs, even with $N_{in} = 0$, the DOA estimation error for Swerling-IV source signals using the proposed method surpasses that of other Swerling sources, excluding Swerling-V. Additionally, as depicted in Fig. 8(b), the DOA estimation error for Swerling-IV source signals consistently outperforms that of other Swerling sources across all SNRs.

The sixth simulation investigates the performance of MBS CS-based DOA estimation in detecting various Swerling source signals across different SNRs, following the same methodology as in the fifth simulation. Each source signal is subjected to a single beam, with N_{bs} set to 1. Four distinct Swerling source signals are considered, with element-space DOA estimation error for Swerling-V included in the figures as a reference, where N_{in} is set to 0. Fig. 9 presents the results of the DOA estimation error. It is evident from this figure that setting N_{in} to 50 reduces the DOA estimation error by approximately 66% for all Swerling source signals compared to $N_{in} = 0$. Moreover, as observed in Fig. 9(b), the DOA estimation error for Swerling-IV is consistently lower than that for other Swerling source signals.

In the seventh simulation, we evaluate the performance of ES, FBS, and multiple-beam beamspace (MBS) compressive sensing (CS)-based direction of arrival (DOA) estimation as the signal-to-noise ratio (SNR) varies for different Swerling source signals. Two source signals are assumed to impinge on the sparse array from DOAs of 60° and 120°. The SNR is varied from −5 dB to 10 dB, with the number of integrated snapshots, N_{in}, set to both 0 and 50. Element-space DOA estimation error for Swerling-V is included in the figures as a reference, with N_{in} set to 0 in this case. The results are presented in Figs. 10 and 11. It is evident that increasing N_{in} to 50 snapshots enhances DOA estimation accuracy by at least 50% compared to $N_{in} = 0$ for all Swerling source signals. Moreover, the proposed MBS CS-based DOA estimation technique consistently outperforms both ES and FBS techniques, reducing the DOA estimation error by over 66% with $N_{in} = 50$ compared to $N_{in} = 0$, across all Swerling source signals.

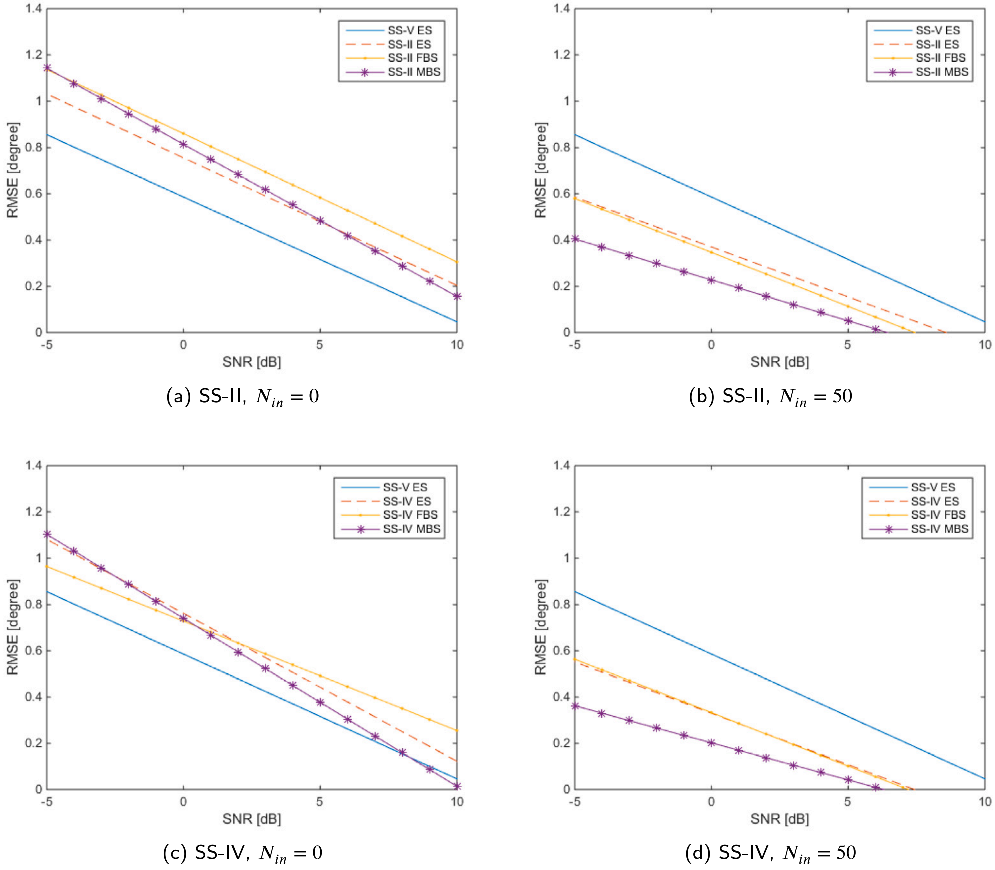

(a) SS-II, $N_{in} = 0$ (b) SS-II, $N_{in} = 50$

(c) SS-IV, $N_{in} = 0$ (d) SS-IV, $N_{in} = 50$

Fig. 11. Performance of CS-based DOA estimate for two source signals when SNR is changed at DOAs of 60° and 120°, $N_{in} = 0$ and 50, Swerling-II and -IV source signals, using ES, FBS, and MBS.

In the seventh simulation, the performance of the ES, FBS, and MBS CS-based DOA estimation is evaluated as the SNR varies for different Swerling source signals. Two source signals are assumed to impinge on the sparse array from DOAs of 60° and 120°. The SNR is varied from −5 dB to 10 dB, with the number of integrated snapshots, N_{in}, set to both 0 and 50. Element-space DOA estimation error for Swerling-V is included in the figures as a reference, with N_{in} set to 0 in this case. The results are demonstrated in Figs. 10 and 11. It is notable that increasing the number of integrated snapshots, N_{in}, to 50 enhances DOA estimation accuracy by at least 50% compared to $N_{in} = 0$ for all Swerling source signals. Furthermore, the proposed MBS CS-DOA estimation technique outperforms both ES and FBS techniques for all Swerling source signals, reducing the DOA estimation error by more than 66% with $N_{in} = 50$ compared to $N_{in} = 0$.

The impact of altering the angular spacing among the various Swerling source signals is examined in the eighth simulation. Consideration is given to two source signals for examination, with the first source signal maintained at a constant DOA of 60°, while the DOA of the second source signal varies from 62° to 90° in 2° increments. The SNR is set to 20 dB, and 10 snapshots are considered for the simulation, with 100 trials conducted for each observation point. Fig. 12 illustrates the angular separation versus the RMSE for various Swerling source signals, with the RMSE versus the angular separation of the Swerling-V source signal provided as a reference. From this figure, it is evident that the error of DOA estimation for angular separations $< 10°$ is higher compared to that for separations $\geq 10°$ for ES, FBS, and MBS techniques. Notably, the DOA estimation error for Swerling-I and -III with angular separations $< 10°$ using the ES technique is higher than that for FBS or MBS. It should be highlighted that the DOA estimation error for applying the MBS technique for all Swerling source signals with angular separations $\geq 10°$ is $< 0.2°$, while that using ES or FBS is $\leq 0.5°$.

In the ninth simulation, the probability of detection (P_d) has been investigated for various Swerling source signals utilising CS-based DOA estimation techniques such as ES, FBS, and MBS. Specifically, consideration is given to two source signals arriving at the sensor array from angles of 60° and 120°. The number of snapshots is fixed at 10, while the SNR is varied. The measurement scenario for P_d is defined as follows: in each iteration, the measured peak heights of the estimated source signals are recorded. If the peak height is ≥ -50 dB, the peak is considered for possible source signal detection; otherwise, the peak is considered as false. This process is repeated 100 times for each SNR value. The P_d obtained for various Swerling source signals, considering various

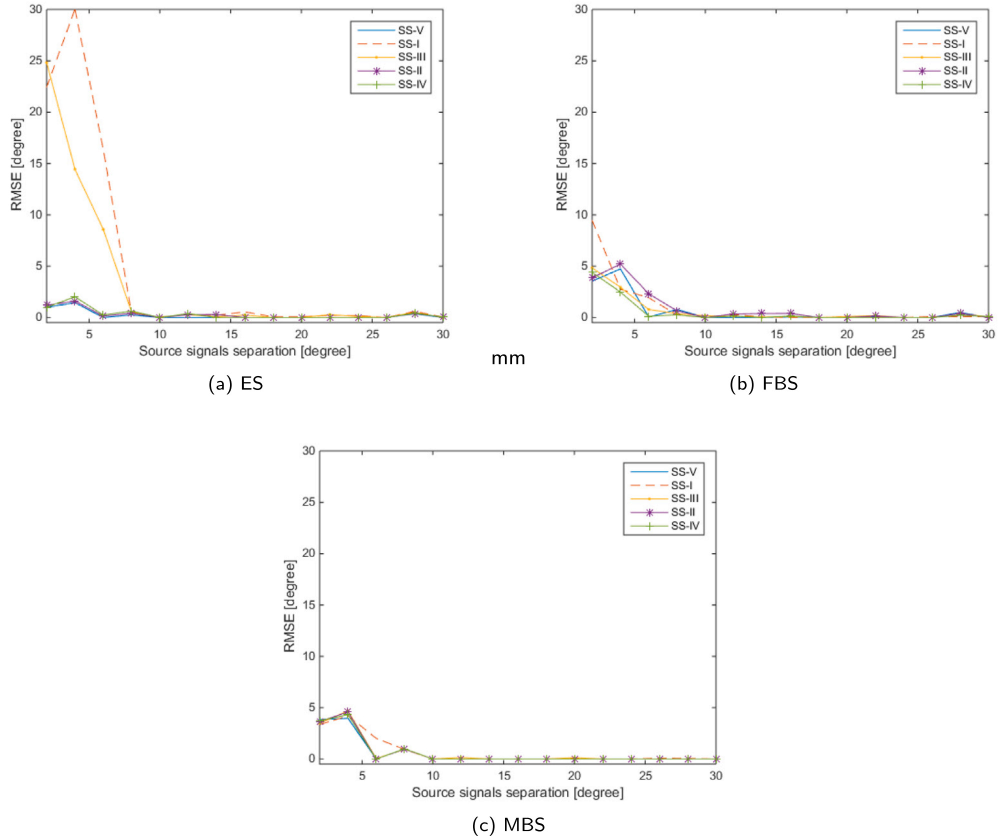

Fig. 12. The estimation error in DOA computation for two sources as a function of separation among the two Swerling source signals, SNR = 20 dB, 10 snapshots, using beamspace and ES algorithms.

integration values, is depicted in Fig. 13. It is notable from this figure that Swerling-I and -III sources require a higher number of signals to be integrated to achieve a higher detection probability than that needed for Swerling-II and -IV source signals using ES or beamspace algorithms. For Swerling-I and -III source signals, by setting the number of integrated signals, N_{in}, to be 100, a satisfactory detection probability can be achieved using the ES technique, as shown in Fig. 13(a, b). However, $N_{in} = 200$ leads to a higher detection probability using the FBS technique, as illustrated in Fig. 13(c, d). The situation is not the same for the MBS technique; to achieve a higher detection probability for Swerling-I sources, N_{in} is set to be 200, while for Swerling-III, $N_{in} = 50$ yields higher detection probability, as evident from Fig. 13(e, f).

4.4. Investigation of moving source signals

Following Swerling moving source signals are investigated. ES, FBS, and MBS algorithms are utilised to study the effect of fluctuating source signals using each of the proposed techniques. All different types of Swerling sources, including the Swerling-V type, are considered to examine the proposed CS-based DOA estimation methods. The simulations aim to investigate two important aspects. The first one is the computational cost of each proposed technique, while the second aspect is the capability of each proposed method to track moving source signals in different scenarios. Accordingly, we consider two uncorrelated equi-power moving source signals. In the forthcoming simulations, we examine three distinct scenarios. The first scenario assumes that the two sources are moving in the same direction, this scenario is noted as *same*. In the second scenario, the two source signals are moving in opposite directions, which is mentioned as *opp*. In the third scenario, one of the source signals is fixed while the other one is moving, denoted as *one & one*. The trajectory of each moving source signal is partitioned into four sections. The first section corresponds to a sinusoidal trajectory followed by the source signal, while the second section represents a stationary source. In the last two sections.

In the tenth simulation, the rank-one update of (20) is used for all moving source signals simulations where the first 10 snapshots are being used for the initial covariance matrix estimate, $\hat{R}_{xx}$, and SNR is chosen to be 10 dB. For Swerling-II fluctuating source signals simulations, N_{in} is chosen to be 10. Fig. 14 illustrates the trajectory of the assumed two fluctuating moving source signals using the three proposed techniques along with different Swerling source signal types. We have omitted the presented results to be only as shown in this figure. However, the same results can be obtained using the different proposed techniques applied to any Swerling source signals model. From the figure, the observed results indicate that the various DOA estimation techniques based

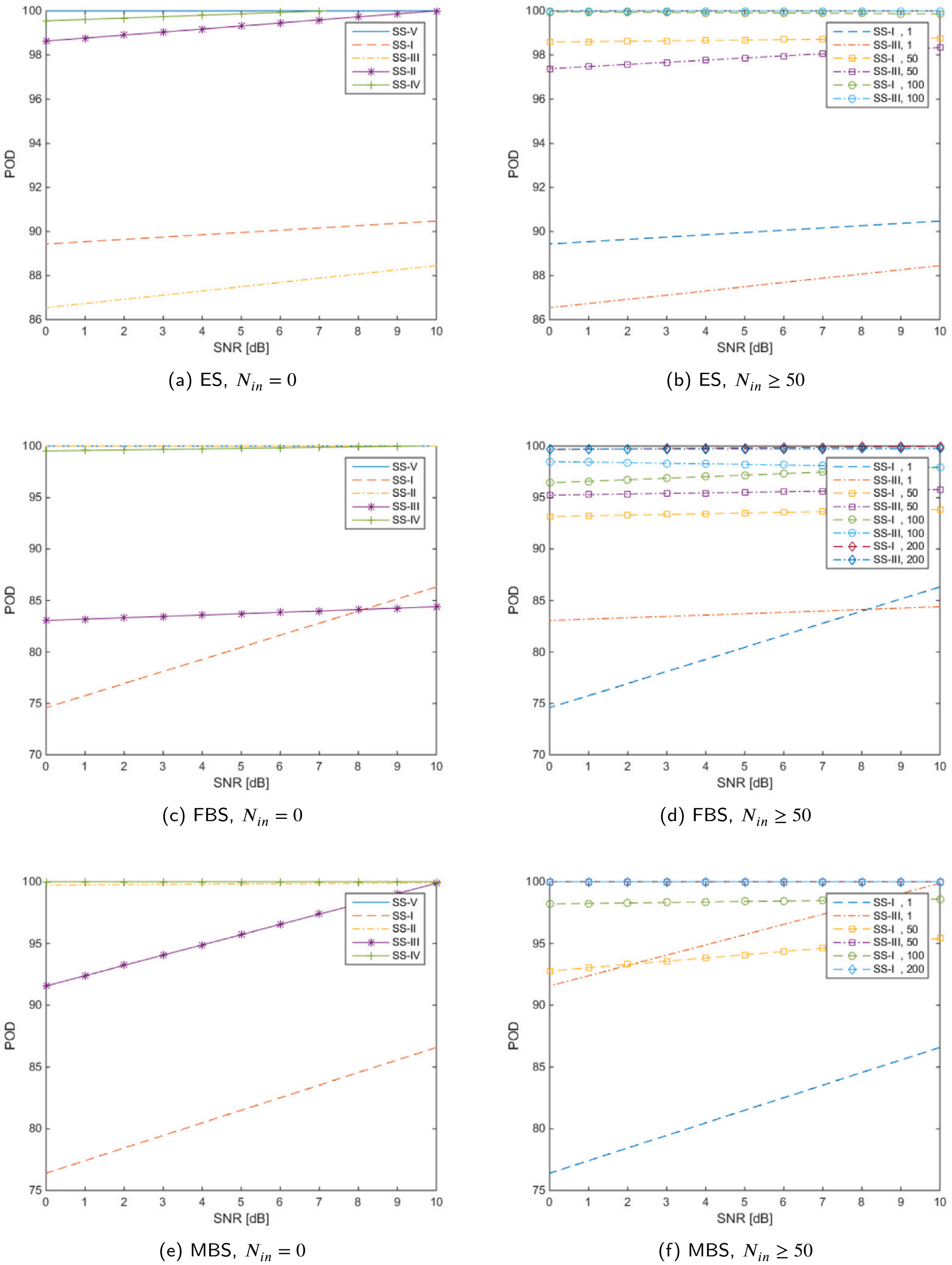

Fig. 13. Probability of detection (POD) for distinct Swerling source signals, specifically two source signals with DOA of 60° and 120°, 10 snapshots, utilising ES, FBS, and MBS algorithms.

on CS exhibit the capability to detect and track the moving fluctuating source sources. Also, it is clear that non-fluctuating source signals can be detected and tracked without any signal integration. Furthermore, in order to be able to detect and track the different Swerling source signals, the received signals must be integrated. From our simulations, it was found that for Swerling-II and -IV $N_{in} = 10$ is enough to accomplish the tracking while for Swerling-I and -III, N_{in} should be set to 100 in order to be able to successfully perform the tracking task.

In the eleventh simulation, we investigate the computational intricacies of DOA estimation techniques based on CS. Specifically, we focus on the ES, FBS, and MBS methods. To quantify this complexity, we employ CPU time as a metric for measurement.

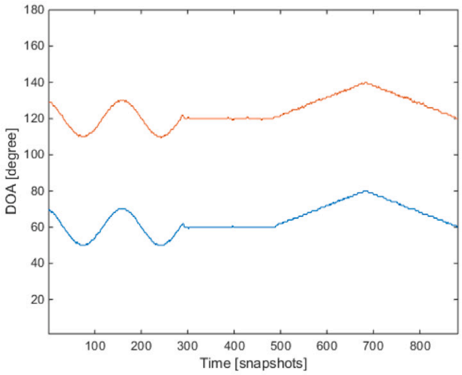

(a) ES - II

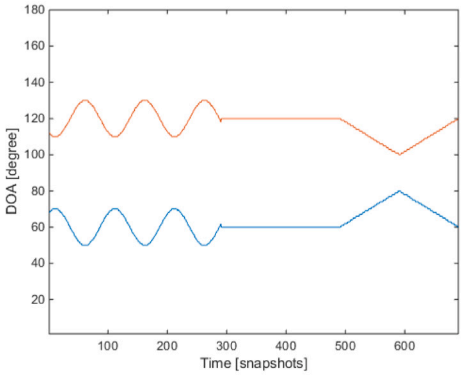

(b) FBS - I

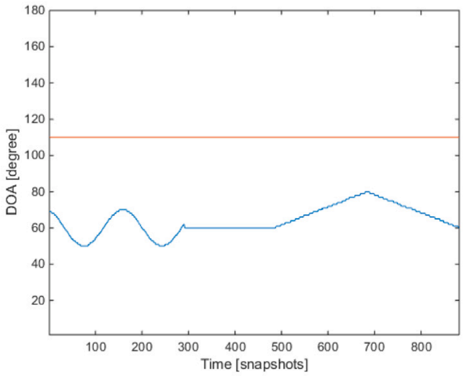

(c) MBS - IV

Fig. 14. Trajectory of two fluctuating source signals using ES CS-based DOA estimation technique. Swerling-II (a) same direction, ES, Swerling-II, N_{in} = 10, SNR = 10 dB, (b) opposite direction, FBS, Swerling-I, N_{in} = 10, SNR = 100 dB, and (c) one fixed and one moving, MBS, Swerling-IV, N_{in} = 10, SNR = 10 dB.

Fig. 15 illustrates the CPU time for ES, FBS, and MBS for different Swerling sources using the three assumed moving source signals trajectories. As can be seen from this figure, the ES technique is the most time-consuming while MBS is the least. To be more clear, Fig. 16 presents the CPU time for Swerling-V source signals using ES, FBS, and MBS. From this figure, it is clear that, for the first trajectory scenario, the MBS technique's computational difficulty is reduced by more than 35% than that of the ES technique (The theoretical computational complexity analysis is also derived in Appendix A.2). The theoretical analysis reveals that the percentage reduction in computational complexity aligns closely with the results observed in the experimental analysis. . For the second trajectory scenario, it is reduced by around 30%, and for the third scenario, it is reduced by around 25%.

According to the findings from the preceding simulations, it is evident that the MBS method for DOA estimation, based on CS, exhibits superior performance compared to the ES and FBS techniques. This observation can be deduced from Figs. 10, 11, 12, 15, and 16. Consequently, for the remainder of the paper, the ES and FBS DOA estimation techniques will be excluded from further consideration.

4.5. Limitations and practical considerations

While the proposed BS weighted-CSKF algorithm exhibits robust performance in DOA estimation and tracking, several limitations warrant consideration. The algorithm's reliance on sufficient SNR levels restricts its efficacy in high-noise or interference-prone environments, with notable performance degradation below specific SNR thresholds. Additionally, the number of sources that can be reliably tracked is constrained, especially in scenarios involving closely spaced or rapidly moving targets. Movement dynamics impose further constraints on angular velocity and acceleration, limiting the algorithm's applicability in highly dynamic settings. Real-time operation demands significant computational resources and strict adherence to specific signal model assumptions, such as far-field sources and independent signals, which may not hold in all scenarios. Moreover, the beamspace transformation introduces a trade-off between computational efficiency and angular resolution. These constraints define the operational boundaries of the algorithm, presenting opportunities for future research to explore adaptive techniques, improved motion models, and hybrid processing methods to address these challenges and expand its applicability.

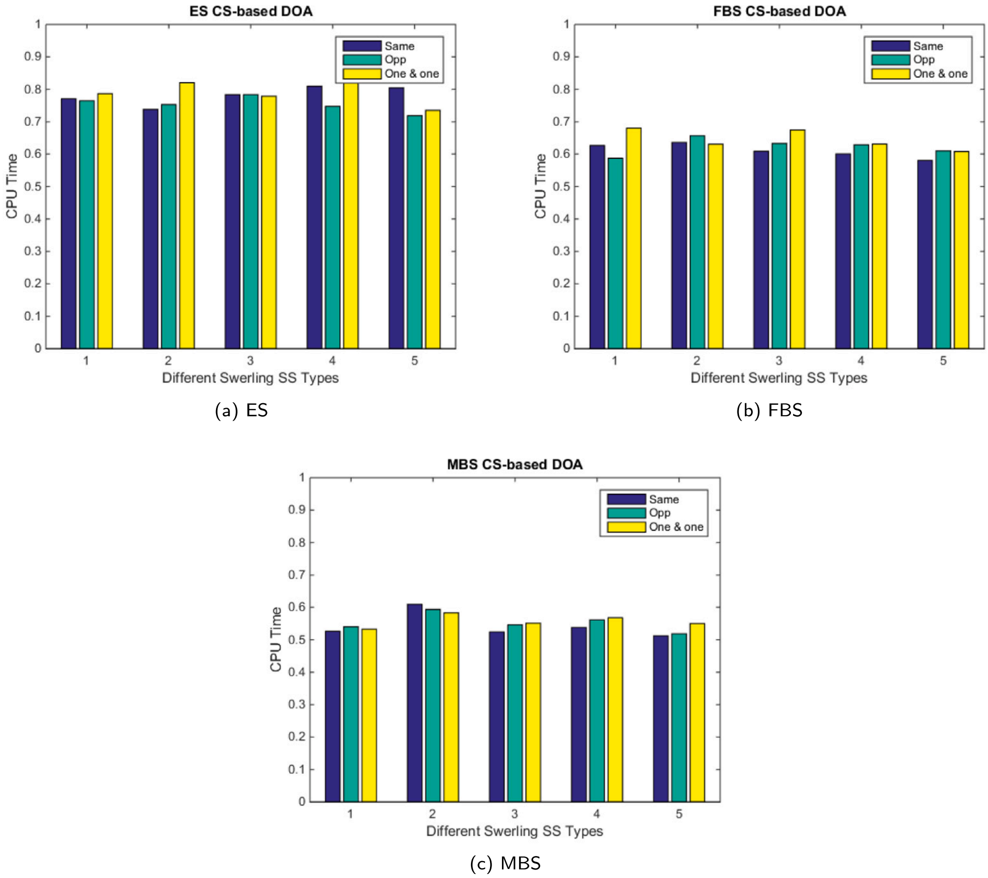

Fig. 15. The computational difficulty of the proposed CS-based DOA computation techniques for the various Swerling-V source signals can be assessed using CPU time as a metric. (a) Element-space; (b) Full beamspace; and (c) Multi-beam beamspace.

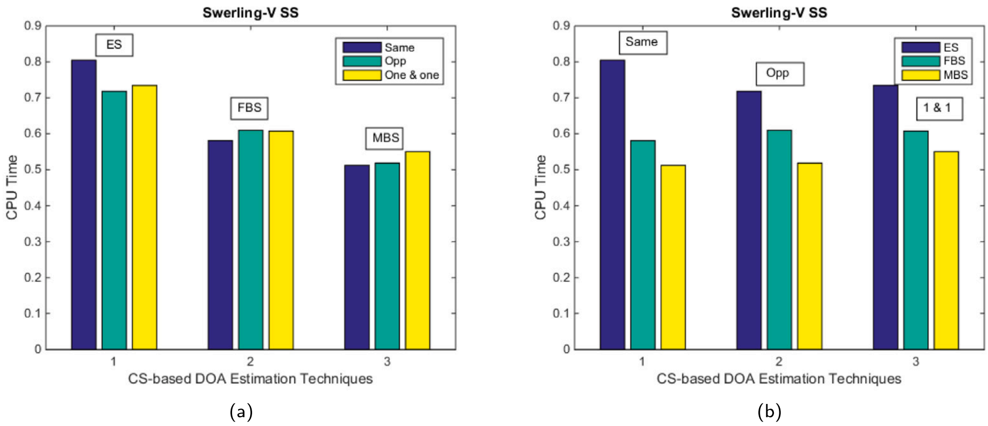

Fig. 16. The computational difficulty of the proposed CS-based DOA computation techniques for the Swerling-V source signal can be assessed using CPU time as a metric. (a) CPU time versus the proposed techniques; and (b) CPU time versus the source signal trajectory.

5. Conclusions

This paper introduces innovative methods within a compressive sensing framework applied to a sparsely arranged linear array. The study presents three distinct techniques in the beamspace domain: full beamspace, reduced-dimension beamspace, and multiple-beam beamspace. Extensive analysis and comparison have been conducted to evaluate the performance of these suggested algorithms in comparison to the conventional element-space technique. Additionally, a rank-one update approach is employed in the compressive sensing framework to update the on-time covariance matrix for DOA estimation. The suggested techniques in this study do not rely on any pre-existing information regarding the number of source signals. These algorithms can accurately estimate the DOA even with a reduced number of snapshots. They can also be utilised to estimate source signals with spatial linkages and associated signals. Using the developed algorithms, we can achieve high-resolution source signal identification with an array of sensors of order $O(M^2)$. Specifically, our methods can recognise source signals with a high accuracy of $O(M)$. Furthermore, utilising the proposed techniques, we can effectively estimate fluctuating source signals. Experimental results indicate that the performance of the multiple-beam beamspace technique, as proposed, surpasses both the full beamspace and element-space techniques in terms of DOA estimation. Besides, using the multiple-beam beamspace technique, the computational load has been reduced by more than 35% than that of the classical element-space technique. Special moving source signals trajectories are studied, and it is shown that the proposed BS weighted-CSKF can distinguish the different source signals for which paths are intersected with each other.

CRediT authorship contribution statement

Amgad A. Salama: Writing – original draft, Data curation, Conceptualization. **Mahmoud A. Shawky:** Resources, Project administration, Methodology, Formal analysis. **Samy H. Darwish:** Writing – review & editing, Investigation. **Adham A. Elmahallawy:** Software, Methodology. **Mohamed Abd Elaziz:** Writing – review & editing, Resources, Methodology. **Ahmad Almogren:** Writing – review & editing, Visualization, Validation, Formal analysis. **Ahmed Gamal Abdellatif:** Writing – review & editing, Formal analysis. **Syed Tariq Shah:** Writing – review & editing, Validation, Supervision, Conceptualization.

Declaration of competing interest

The authors declare that they have no known competing financial interests or personal relationships that could have appeared to influence the work reported in this paper.

Acknowledgement

This work was supported by King Saud University, Riyadh, Saudi Arabia, through Researchers Supporting Project number (RSP2024R184).

Appendix

The appendices referenced in this manuscript are detailed below.

A.1. Cramér-Rao lower bound analysis for beamspace compressed sensing scenarios

To establish the theoretical performance limits of the proposed DOA estimation method, we derive the Cramér-Rao Lower Bound (CRLB) for our beamspace compressed sensing scenario. The CRLB provides a lower bound on the variance of any unbiased estimator, serving as a benchmark for evaluating estimator efficiency.

- *Step 1 (Signal model in beamspace domain)*: Consider our beamspace measurement model as follows.

$$\mathbf{y}_{bs} = \mathbf{B}^H \mathbf{y} = \mathbf{B}^H \mathbf{A}(\theta)\mathbf{s} + \mathbf{B}^H \mathbf{n} \tag{23}$$

  where $\mathbf{B}^H$ is the beamspace transformation matrix, $\mathbf{A}(\theta)$ is the array steering matrix, $\mathbf{s}$ contains the source signals, and $\mathbf{n}$ is complex Gaussian noise.
- *Step 2 (Fisher information matrix)*: For our scenario with L sources and K snapshots, the Fisher Information Matrix (FIM) elements for the unknown parameters θ_i and θ_j are given by:

$$[\mathbf{F}]_{i,j} = 2K \cdot Re\left\{ tr\left[\mathbf{R}_{bs}^{-1} \frac{\partial \mathbf{R}_{bs}}{\partial \theta_i} \mathbf{R}_{bs}^{-1} \frac{\partial \mathbf{R}_{bs}}{\partial \theta_j} \right] \right\} \tag{24}$$

  where $\mathbf{R}_{bs}$ is the beamspace covariance matrix:

$$\mathbf{R}_{bs} = \mathbf{B}^H \mathbf{A}(\theta)\mathbf{R}_s \mathbf{A}^H(\theta)\mathbf{B} + \sigma^2 \mathbf{B}^H \mathbf{B} \tag{25}$$

  The partial derivatives in the beamspace domain are:

$$\frac{\partial \mathbf{R}_{bs}}{\partial \theta_i} = \mathbf{B}^H \left[\frac{\partial \mathbf{A}(\theta)}{\partial \theta_i} \mathbf{R}_s \mathbf{A}^H(\theta) + \mathbf{A}(\theta)\mathbf{R}_s \frac{\partial \mathbf{A}^H(\theta)}{\partial \theta_i} \right] \mathbf{B} \tag{26}$$

- *Step 3 (CRLB for beamspace DOA estimation)*: The CRLB for the ith source DOA estimate is given by:

$$CRLB(\theta_i) = [\mathbf{F}^{-1}]_{i,i} \tag{27}$$

For high SNR conditions, this can be approximated as:

$$CRLB(\theta_i) \approx \frac{\sigma^2}{2K}\left[\mathbf{P}_i^H \mathbf{B}\mathbf{B}^H \mathbf{P}_i\right]^{-1} \tag{28}$$

where $\mathbf{P}_i = \frac{\partial \mathbf{a}(\theta_i)}{\partial \theta_i}$ is the derivative of the steering vector with respect to θ_i.

- *Step 4 (Effect of compressed sensing)*: The compressed sensing framework modifies the CRLB through the measurement matrix $\boldsymbol{\Phi}$:

$$CRLB_{CS}(\theta_i) = CRLB(\theta_i) \cdot tr\left[(\boldsymbol{\Phi}^H \boldsymbol{\Phi})^{-1}\right] \tag{29}$$

- *Step 5 (Impact of Kalman filtering)*: The recursive nature of the Kalman filter affects the bound through temporal correlation. For our tracking scenario, the modified CRLB becomes:

$$CRLB_{KF}(\theta_i) = \left[\mathbf{F} + \mathbf{Q}^{-1}\right]_{i,i}^{-1} \tag{30}$$

where $\mathbf{Q}$ is the process noise covariance matrix from the Kalman filter state model.

- *Step 6 (Combined bound for BS weighted-CSKF)*: The final CRLB for our proposed BS weighted-CSKF algorithm combines all these effects:

$$CRLB_{total}(\theta_i) = CRLB_{KF}(\theta_i) \cdot \gamma_i \tag{31}$$

where γ_i is the beamspace efficiency factor:

$$\gamma_i = \frac{tr\left[\mathbf{B}^H \mathbf{B}\right]}{tr\left[\mathbf{I}\right]} \cdot tr\left[(\boldsymbol{\Phi}^H \boldsymbol{\Phi})^{-1}\right] \tag{32}$$

This combined bound provides a theoretical lower limit on the achievable estimation accuracy of our algorithm, accounting for the effects of beamspace transformation, compressed sensing, and Kalman filtering.

A.2. Computational complexity analysis

The computational complexity of the proposed BS weighted-CSKF algorithm can be analysed by examining its major components, as follows.

- *Beamspace transformation*: The beamspace transformation involves the multiplication of the input signal by the beamspace transformation matrix:

$$\mathbf{y}_{bs} = \mathbf{B}^H \mathbf{y} \tag{33}$$

For an M-element array with N_{bs} beams, the matrix multiplication cost is $O(MN_{bs})$. This operation is performed for each of the N snapshots. Accordingly, the total complexity for beamspace transformation is $O(MN_{bs}N)$.

- *Covariance matrix computation*: For the rank-one update of the covariance matrix:

$$\mathbf{R}_{xx}(n) = \lambda \mathbf{R}_{xx}(n-1) + (1-\lambda)\mathbf{y}(n)\mathbf{y}^H(n) \tag{34}$$

The computation cost of the matrix update operation is $O(M^2)$, performed once per snapshot. Accordingly, the total complexity for covariance update is $O(M^2N)$.

- *Kalman filter operations*: The Kalman filter involves several matrix operations:

1. *Prediction step*:

$$\hat{\mathbf{s}}_{k+1|k} = \mathbf{A}\hat{\mathbf{s}}_{k|k} \tag{35}$$

$$\mathbf{P}_{k+1|k} = \mathbf{A}\mathbf{P}_{k|k}\mathbf{A}^T + \mathbf{Q} \tag{36}$$

2. *Update step*:

$$\mathbf{K}_k = \mathbf{P}_{k+1|k}\boldsymbol{\Phi}'^T(\boldsymbol{\Phi}'\mathbf{P}_{k+1|k}\boldsymbol{\Phi}'^T + \mathbf{R}_k)^{-1} \tag{37}$$

For grid size K, the matrix multiplications are $O(K^2)$. while the matrix inversion and update operations costs $O(K^3)$ and $O(K^2)$, respectively. Note that the use of beamspace processing reduces these operations by working with a smaller matrix size.

3. *Total complexity*: By combining the cost associated with each component (i.e., Beamspace transformation of order $O(MN_{bs}N)$, Covariance update of order $O(M^2N)$, and Kalman filter operations of order $O(K \log K)$), we get the total computational complexity of order $O(M^2N + MK \log K)$. where M is the number of array elements, N is the number of snapshots, and K is the grid size.

- *Comparison with element-space processing*: In conventional element-space processing, the computational complexity is $O(M^3N + K^3)$. In contrast, our beamspace approach achieves a significant reduction in complexity by leveraging the reduced dimensionality of the processed data, efficient matrix operations within the beamspace domain, and an optimised implementation of the Kalman filter. The 35% reduction in computational load compared to element-space processing can be verified by comparing the complexity terms when typical values are substituted:
$$\frac{O(M^2N + MK\log K)}{O(M^3N + K^3)} \approx 0.65 \tag{38}$$
for practical values of M, N, and K in typical array processing scenarios.

Data availability

No data was used for the research described in the article.

References

[1] Q. Shen, W. Liu, W. Cui, S. Wu, Underdetermined doa estimation under the compressive sensing framework: A review, IEEE Access 4 (2016) 8865–8878.
[2] O.J. Famoriji, T. Shongwe, Critical review of basic methods on doa estimation of em waves impinging a spherical antenna array, Electronics 11 (2) (2022) 208.
[3] B. Li, Y. Zou, Y. Zhu, Direction estimation under compressive sensing framework: A review and experimental results, in: 2011 IEEE International Conference on Information and Automation, 2011, pp. 63–68.
[4] R. Schmidt, Multiple emitter location and signal parameter estimation, IEEE Trans. Antennas Propag. 34 (3) (1986) 276–280.
[5] R. Roy, T. Kailath, Esprit-estimation of signal parameters via rotational invariance techniques, Acoust. IEEE Trans. Speech Signal Process. 37 (7) (1989) 984–995.
[6] D. Malioutov, M. Cetin, A.S. Willsky, A sparse signal reconstruction perspective for source localization with sensor arrays, IEEE Trans. Signal Process. 53 (8) (2005) 3010–3022.
[7] S.T. Shah, M.A. Shawky, J.u.R. Kazim, et al., Coded environments: Data-driven indoor localisation with reconfigurable intelligent surfaces, Commun. Eng. 3 (2024) 66, http://dx.doi.org/10.1038/s44172-024-00209-0.
[8] X. Xu, X. Wei, Z. Ye, DOA estimation based on sparse signal recovery utilising weighted l 1-norm penalty, IEEE Signal Process. Lett. 19 (3) (2012) 155–158.
[9] Q. Wang, H. Yu, J. Li, F. Ji, F. Chen, Sparse bayesian learning using generalized double Pareto prior for DOA estimation, IEEE Signal Process. Lett. 28 (2021) 1744–1748.
[10] A.A. Salama, M.O. Ahmad, M. Swamy, Underdetermined DOA estimation using MVDR-weighted LASSO, Sensors 16 (9) (2016) 1549.
[11] A.A. Salama, M. Morsy, S.H. Darwish, A novel low complexity CS-based DOA estimation technique, in: 2021 International Telecommunications Conference, ITC-Egypt, 2021, pp. 1–4.
[12] J.A. Tropp, Greed is good: Algorithmic results for sparse approximation, IEEE Trans. Inf. Theory 50 (10) (2004) 2231–2242.
[13] A. Aich, P. Palanisamy, On-grid DOA estimation method using orthogonal matching pursuit, in: International Conference on Signal Processing and Communication, ICSPC, 2017, pp. 483–487.
[14] I.F. Gorodnitsky, B.D. Rao, Sparse signal reconstruction from limited data using focuss: A re-weighted minimum norm algorithm, IEEE Trans. Signal Process. 45 (3) (1997) 600–616.
[15] Z. Yang, L. Xie, On gridless sparse methods for multi-snapshot DOA estimation, in: IEEE International Conference on Acoustics, Speech and Signal Processing, ICASSP, 2016, pp. 3236–3240.
[16] A. Das, Real-valued sparse bayesian learning for off-grid direction-of-arrival (DOA) estimation in ocean acoustics, IEEE J. Ocean. Eng. 46 (1) (2020) 172–182.
[17] J. Zhu, Q. Zhang, P. Gerstoft, M.-A. Badiu, Z. Xu, Grid-less variational Bayesian line spectral estimation with multiple measurement vectors, Signal Process. 161 (2019) 155–164.
[18] N. Lee, MAP support detection for greedy sparse signal recovery algorithms in compressive sensing, IEEE Trans. Signal Process. 64 (19) (2016) 4987–4999.
[19] D.P. Wipf, B.D. Rao, S. Nagarajan, Latent variable bayesian models for promoting sparsity, IEEE Trans. Inform. Theory 57 (9) (2011) 6236–6255.
[20] Z. Yang, L. Xie, C. Zhang, A discretization-free sparse and parametric approach for linear array signal processing, IEEE Trans. Signal Process. 62 (19) (2014) 4959–4973.
[21] S.D. Babacan, S. Nakajima, M.N. Do, Bayesian group-sparse modeling and variational inference, IEEE Trans. Signal Process. 62 (11) (2014) 2906–2921.
[22] G. Liang, C. Li, L. Qiu, T. Shen, Y. Hao, State-updating-based DOA estimation using sparse Bayesian learning, Appl. Acoust. 192 (2022) 108719.
[23] P. Pal, P. Vaidyanathan, Nested arrays: A novel approach to array processing with enhanced degrees of freedom, IEEE Trans. Signal Process. 58 (8) (2010) 4167–4181.
[24] A. Moffet, Minimum-redundancy linear arrays, IEEE Trans. Antennas Propag. 16 (2) (1968) 172–175.
[25] W.-K. Ma, T.-H. Hsieh, C.-Y. Chi, DOA estimation of quasi-stationary signals via Khatri–Rao subspace, in: IEEE International Conference on Acoustics, Speech and Signal Processing, ICASSP, 2009, pp. 2165–2168.
[26] M. Wing-Kin, H. Tsung-Han, C. Chong-Yung, DOA estimation of quasi-stationary signals with less sensors than sources and unknown spatial noise covariance: A Khatri–Rao subspace approach, IEEE Trans. Signal Process. 58 (4) (2010) 2168–2180.
[27] Y.D. Zhang, M.G. Amin, B. Himed, Sparsity-based DOA estimation using co-prime arrays, in: IEEE International Conference on Acoustics, Speech and Signal Processing, ICASSP, 2013, pp. 3967–3971.
[28] K. Adhikari, J.R. Buck, K.E. Wage, Beamforming with extended co-prime sensor arrays, in: IEEE International Conference on Acoustics, Speech and Signal Processing, ICASSP, 2013, pp. 4183–4186.
[29] Q. Shen, W. Liu, W. Cui, S. Wu, Y.D. Zhang, M.G. Amin, Low-complexity direction-of-arrival estimation based on wideband co-prime arrays, IEEE/ACM Trans. Audio Speech Lang. Process. 23 (9) (2015) 1445–1456.
[30] P. Rocca, G. Oliveri, R.J. Mailloux, A. Massa, Unconventional phased array architectures and design methodologies—a review, Proc. IEEE 104 (3) (2016) 544–560.
[31] L. Li, F. Gong, S. Liu, Semi-supervised learning method for source range estimation in shallow water, J. Phys. Conf. Ser. 2458 (1) (2023).
[32] Q. Wang, H. Yu, J. Li, F. Ji, F. Chen, Adaptive grid refinement method for DOA estimation via sparse Bayesian learning, IEEE J. Ocean. Eng. 48 (3) (2023) 806–819.

[33] Y. Zhou, C. Sun, L. Xie, A trajectory-oriented possion multi-Bernoulli mixture method for matched field tracking to achieve trajectory continuity, in: IEEE in OCEANS 2022-Chennai, 2022, pp. 1–4.
[34] S. Liu, G. Trenkler, Hadamard Khatri–Rao, Kronecker and other matrix products, Int. J. Inform. Syst. Sci. 4 (1) (2008) 160–177.
[35] M. Hyder, K. Mahata, An approximate $l0$ norm minimization algorithm for compressed sensing, in: IEEE International Conference on Acoustics, Speech and Signal Processing, ICASSP, 2009, pp. 3365–3368.
[36] C.R. Berger, J. Areta, K. Pattipati, P. Willett, Compressed sensing-a look beyond linear programming, in: IEEE International Conference on Acoustics, Speech and Signal Processing, ICASSP, 2008, pp. 3857–3860.
[37] L. Mancera, J. Portilla, $l0$-Norm-based sparse representation through alternate projections, in: International Conference on Image Processing, ICIP, vol. 2092, 2006.
[38] G.H. Mohimani, M. Babaie-Zadeh, C. Jutten, Fast sparse representation based on smoothed $l0$ norm, in: Independent Component Analysis and Signal Separation, Springer, 2007, pp. 389–396.
[39] E.J. Cand'es, The restricted isometry property and its implications for compressed sensing, C. R. Math. 346 (9) (2008) 589–592.
[40] R. Baraniuk, M. Davenport, R. DeVore, M. Wakin, A simple proof of the restricted isometry property for random matrices, Constr. Approx. 28 (3) (2008) 253–263.
[41] E.J. Cand'es, J. Romberg, T. Tao, Robust uncertainty principles: Exact signal reconstruction from highly incomplete frequency information, IEEE Trans. Inform. Theory 52 (2) (2006) 489–509.
[42] D.L. Donoho, Compressed sensing, IEEE Trans. Inform. Theory 52 (4) (2006) 1289–1306.
[43] E.J. Candes, T. Tao, Near-optimal signal recovery from random projections: Universal encoding strategies, IEEE Trans. Inform. Theory 52 (12) (2006) 5406–5425.
[44] A. Xenaki, P. Gerstoft, K. Mosegaard, Compressive beamforming, J. Acoust. Soc. Am. 136 (1) (2014) 260–271.
[45] V.A. Morozov, On the solution of functional equations by the method of regularization, in: Soviet Math. Dokl, vol. 7, 1966, pp. 414–417.
[46] W.C. Karl, Regularization in image restoration and reconstruction, in: Handbook of Image and Video Processing, 2000, pp. 141–160.
[47] R. Tibshirani, Regression shrinkage and selection via the LASSO, J. R. Stat. Soc. Ser. B Stat. Methodol. (1996) 267–288.
[48] S.S. Chen, D.L. Donoho, M.A. Saunders, Atomic decomposition by basis pursuit, SIAM J. Sci. Comput. 20 (1) (1998) 33–61.
[49] P.S. Maybeck, G.M. Siouris, Stochastic models, estimation, and control, volume I, IEEE Trans. Syst. Man Cybern. 10 (5) (1980) 282-282.
[50] S.J. Julier, J.J. LaViola, On kalman filtering with nonlinear equality constraints, IEEE Trans. Signal Process. 55 (6) (2007) 2774–2784.
[51] A. Carmi, P. Gurfil, D. Kanevsky, Methods for sparse signal recovery using kalman filtering with embedded pseudo-measurement norms and quasi-norms, IEEE Trans. Signal Process. 58 (4) (2010) 2405–2409.
[52] P.C. Hansen, D.P. O'Leary, The use of the l-curve in the regularization of discrete ill-posed problems, SIAM J. Sci. Comput. 14 (6) (1993) 1487–1503.
[53] P.C. Hansen, T.K. Jensen, G. Rodriguez, An adaptive pruning algorithm for the discrete l-curve criterion, J. Comput. Appl. Math. 198 (2) (2007) 483–492.
[54] M. Grant, S. Boyd, CVX: Matlab software for disciplined convex programming, version 2.1, 2014.
[55] M.C. Grant, S.P. Boyd, Graph implementations for non-smooth convex programs, in: V.D. Blondel, S.P. Boyd, H. Kimura (Eds.), Recent Advances in Learning and Control, in: Lecture Notes in Control and Information Sciences, vol. 371, Springer, London, 2007, pp. 95–110.
[56] R.H. Tütüncü, K.C. Toh, M.J. Todd, Solving semidefinite-quadratic-linear programs using sdpt3, Math. Program. 95 (2) (2003) 189–217.
[57] P. Stoica, P. Babu, J. Li, New method of sparse parameter estimation in separable models and its use for spectral analysis of irregularly sampled data, IEEE Trans. Signal Process. 59 (1) (2010) 35–47.
[58] P. Babu, P. Stoica, Connection between spice and square-root lasso for sparse parameter estimation, Signal Process. 95 (2014) 10–14.
[59] X. Tan, W. Roberts, J. Li, P. Stoica, Sparse learning via iterative minimization with application to mimo radar imaging, IEEE Trans. Signal Process. 59 (3) (2010) 1088–1101.